Surface Plasmon Resonance sensor showing enhanced sensitivity for CO_2 detection in the mid-infrared range

Sylvain Herminjard[1]*, **Lorenzo Sirigu**[1], **Hans Peter Herzig**[1], **Eric Studemann**[2], **Andrea Crottini**[2], **Jean-Paul Pellaux**[2], **Tobias Gresch**[3], **Milan Fischer**[3] **and Jérôme Faist**[3]

[1]*Institute of Microtechnology, University of Neuchâtel, CH-2000 Neuchâtel, Switzerland*
[2]*Hach Ultra Analytics, CH-1222 Vésenaz, Switzerland*
[3]*Institute for Quantum Electronics, ETH-Zürich, CH-8093 Zürich, Switzerland*
Corresponding author: sylvain.herminjard@unine.ch

Abstract: We present the first optical sensor based on Surface Plasmon Resonance (SPR) operating in the mid-infrared range. The experimental setup is based on a Kretschmann geometry with Ti/Au layers deposited on a CaF_2 prism where light excitation is provided by a Quantum Cascade Laser (QCL) source. Evidence of SPR is presented and the sensing capability of the system is demonstrated by using CO_2 and N_2 mixtures as test samples. Due to the absorption of CO_2 at this wavelength, it is shown that the sensitivity of this configuration is five times higher than a similar SPR sensor operating in the visible range of the spectrum.

OCIS codes: (240.6680) Surface plasmons; (280.4788) Optical sensing and sensors; (040.3060) Infrared; (140.5965) Semiconductor lasers, quantum cascade; (250.5403) Plasmonics

---

References and links

1. J. Homola, S. S. Yee and G. Gauglitz, "Surface plasmon resonance sensors: review," Sens. Actuators B **54,** 3–15 (1999).
2. Z. Salamon and G. Tollin, "Surface plasmon resonance, theory," Encyclopedia of Spectroscopy and Spectrometry, 2311-2319 (2000).
3. E. Kretschmann and H. Raether, "Radiative decay of non radiative surface plasmons excited by light," Zeitschrift Fur Naturforschung Part A-Astrophysik Physik Und Physikalische Chemie **A 23,** 2135–2136 (1968).
4. D. C. Cullen, R. G. W. Brown and C. R. Lowe, "Detection of immuno-complex formation via surface-plasmon resonance on gold-coated diffraction gratings," Biosensors **3,** 211–225 (1987).
5. R. C. Jorgenson and S. S. Yee, "Detection of immuno-complex formation via surface-plasmon resonance," Sens. Actuators B **12,** 213–220 (1993).
6. M. Born and E. Wolf, "Elementary theory of dispersion," in *Principles of Optics, 7th Edition,* (University Press, Cambridge, 1999), pp. 95–103.
7. A. Hanning, J. Roeraade, J. J. Delrow and R. C. Jorgenson, "Enhanced sensitivity of wavelength modulated surface plasmon resonance devices using dispersion from a dye solution," Sens. Actuators B **54,** 25–36 (1999).
8. S. Herminjard, A. Crottini, L. Vaccaro, H-P. Herzig, E. Studemann, G.M. Nicolle, "Surface plasmon waveguide resonance spectroscopy applied on food dyes solutions under anomalous dispersion," presented at the EOS Topical Meeting on Molecular Plasmonic Devices, Engelberg, Switzerland, 27–29 April 2006.
9. B. H. Stuart, *Infrared spectroscopy : fundamentals and applications* (Wiley, Chichester, 2004).
10. W. Shin, M. Matsumiya, F. Qiu, N. Izu and N. Murayama, "Thermoelectric gas sensor for detection of high hydrogen concentration," Sens. Actuators B **97,** 344–347 (2004)
11. K. Takeuchi, T. Tanaka, M. Ikeda, K. Shibata, Y. Sakauchi, Y. Yamada and S. Nakano, "Highly accurate CO_2 gas sensor using a modulation-type pyroelectric infrared detector," Jpn. J. Appl. Phys. **32,** 221–227 (1993).

---

12. M. W. Sigrist, "Trace gas monitoring by laser-photoacoustic spectroscopy," Inf. Phys. Technol. **36,** 415–425 (1995).
13. J. Faist, F. Capasso, D. L. Sivco, C. Sirtori, A. L. Hutchinson and A. Y. Cho, "Quantum cascade laser," Science **264,** 553–556 (1994).
14. H. Raether, "Surface plasmons on smooth and rough surfaces and on gratings," Springer tracts in moderns physics **111,** Springer, Berlin (1988).
15. W. Knoll, "Interfaces and thin films as seen by bound electromagnetic waves," Annu. Rev. Phys. Chem. **49,** 569–638 (1998).
16. J. Worm, "Winspall 2.20 software", 2001, http://www.mpip-mainz.mpg.de/ johanns/winspall2.ZIP.
17. E. D. Palik, *Handbook of optical constants of solids II* (Academic Press, San Diego, 1991)
18. M. A. Ordal, L. Long, R. J. Bell, S. E. Bell, R. R. Bell, R. W. Alexander and C. A. Ward, "Optical properties of the metals Al, Co, Cu, Au, Fe, Pb, Ni, Pd, Pt, Ag, Ti, and W in the infrared and far infrared," Appl. Opt. **22,** 1099–1119 (1983).
19. B. Liedberg, C. Nylander and I. Lundstrom, "Biosensing with surface-plasmon resonance - how it all started," Biosens. Bioelectron. **10,** 1–9 (1995).
20. E. Rosencher and V. Borge, *Optoélectronique, 2nd edition* (Dunod, Paris, 2002), pp. 316–319.
21. Y. Clergent, C. Durou and M. Laurens, "Refractive index variations for argon, nitrogen, and carbon dioxide at $\lambda = 632.8$ nm (He-Ne laser light) in the range 288.15 K $\leq T \leq$ 323.15 K, $0 < p < 110$ kPa," Journal Of Chemical And Engineering Data **44,** 197–199 (1999).
22. G. J. Ashwell and M. P. S. Roberts, "Highly selective surface plasmon resonance sensor for NO_2," Electronics Letters **32,** 2089–2091 (1996).
23. G. P. Luo, C. Peng, H. Q. Le, S. S. Pei, W.-Y. Hwang, B. Ishaug, J. Um, J. N. Baillargeon and C.-H. Lin, "Grating-tuned external-cavity quantum-cascade semiconductor lasers," Appl. Phys. Lett. **78,** 2834–2836 (2001).

1. Introduction

Surface plasmon based optical sensors have attracted a great interest in the last 10 years mostly for biochemical or biomedical applications. Refractive index variations in the probed optical medium are rapidly observed with surface-plasmon-based techniques providing a high sensitivity that is hardly achieved with other optical techniques [1].

Surface Plasmons (SP) are charge-density oscillations localized at the interface between a metallic film (active layer) and a dielectric surface [2]. Surface Plasmon Resonance (SPR) refers to the optical excitation of these charge-density oscillations. There are various methods that use different coupling devices between the incident light and the SP. The most widely used method is the Kretschmann geometry where the metallic film is coated directly on a prism [3] or on a plate held on a prism with an appropriate index matching liquid. Other coupling methods include the use of diffraction gratings [4] or optical fibers [5], which are more complex to design and realize.

SPR is very sensitive to variations of the refractive index of the medium located next to the active layer while the refractive index of this measured medium is probed by the SP. Variations of 10^{-5} RIU (Refractive Index Units) can be measured with systems operating in the visible spectrum [1]. Nevertheless, this technique gives information only on the refractive index variation of the probed medium without any selectivity on its components. On the other hand the sensor sensitivity can be enhanced by using anomalous dispersion properties [6] of the measured medium. This approach has been successfully demonstrated in ref [7] for wavelength interrogated SPR sensors. More recently, we showed in the visible range that absorption can play a direct role for angle interrogated SPR sensor [8]. In this previous work, we measured variations of concentration of food dyes solutions close to absorption at three different wavelengths in the visible range. We showed that the sensitivity was higher at a wavelength located near an absorption peak of the food dye solution.

So far, SPR has been exploited only in the visible and near-infrared spectral region due to the wide availability of optical materials and efficient light sources and detectors. Nevertheless, most of the optical absorption spectral lines associated to the vibrational frequencies of gas molecules take place in the mid-infrared portion of the optical spectrum [9]. These absorption

characteristics allow to design selective gas sensors using thermoelectric, pyroelectric or photoacoustic detectors in the mid-infrared range [10][11][12]. These sensors are mainly based on optical transmission or absorption measurements; high sensitivity is obtained provided that the medium is probed over long optical paths or large volumes. In contrast to this, SPR technique, sampling the few hundred nanometers-thick analyte close to the sensor surface, is extremely effective when limited volumes are available or high compactness is required. The aim of this work is to extend SPR techniques to mid-IR wavelengths, thus adding to a a surface probe the sensitivity advantage of an interrogation based on optical absorption. In order to access this spectral window, we developed a SPR-based optical sensor by combining a Quantum Cascade Laser (QCL) [13] as mid-infrared light source with a metallized CaF_2 coupling prism. In this work, we present evidence that surface plasmon resonance with this mid-infrared optical setup is obtained and we address the sensing capability of the system by measuring various mixtures of carbon dioxide (CO_2) and nitrogen (N_2).

2. Principles and experiments

Surface plasmon resonance (SPR) is a charge density wave which takes place at the interface of two media with dielectric constants of opposite signs like, for example, a metal and a dielectric. This charge density wave is associated with a TM electromagnetic wave and whose field vector is at maximum at the interface and decays evanescently into the adjacent media. The propagation constant of this surface plasma wave is given by the following expression :

$$\mathbf{K_{sp}} = k_0 \sqrt{\frac{\varepsilon_m \varepsilon_d}{\varepsilon_m + \varepsilon_d}} = \frac{2\pi}{\lambda_0} \sqrt{\frac{\varepsilon_m \varepsilon_d}{\varepsilon_m + \varepsilon_d}}, \tag{1}$$

where ε_m and ε_d are the complex dielectric constants of the metal and the dielectric [14]. This wave can be optically excited by using a coupling prism coated with a thin metal layer (Kretschmann prism configuration), where a TM-polarized light beam is impinging on the metallized face of the prism through the prism itself under total internal reflection conditions. In order to get the coupling requirement, the horizontal component of the incident light wavevector, k_x, has to match the real part of the SP wavevector, Re$\{\mathbf{K_{sp}}\}$, given by eq. (1). This resonance condition is obtained by using an appropriate optical coupling device, otherwise the horizontal wavevector of the incident light in free space is smaller than the real part of the SP wavevector and the resonance condition is not met [15]. At the resonance angle, a resonant transfer of energy takes place between the optical wave and the surface plasma wave. While illuminating the prism with a light beam with a certain angular distribution, the intensity profile of the reflected light shows a clear sharp dip located at the angle of resonance, as shown in Fig. 1. The resonance linewidth strongly depends on the excitation wavelength, the metal layer structure and the refractive index of the dielectric medium surrounding this layer. These refractive index variations modify significantly the SPR conditions, varying the resonance angle value and therefore the resonance angular position. The refractive index variations are therefore inferred by the spatial displacement of the resonance peak. These features allow SPR-based devices to be used as high sensitivity optical sensors. In order to have access to the optical absorption windows of interest (fingerprints) for gas spectroscopy, SPR must be extended to the mid-infrared region of the optical spectrum. For example, if CO_2 needs to be measured, the system should be designed at a wavelength close to an absorption peak of CO_2. For this purpose, we selected the vibrational absorption peak of CO_2 located close to 4.3 μm and we performed simulations in order to design a suitable structure able to exhibit SPR at this wavelength.
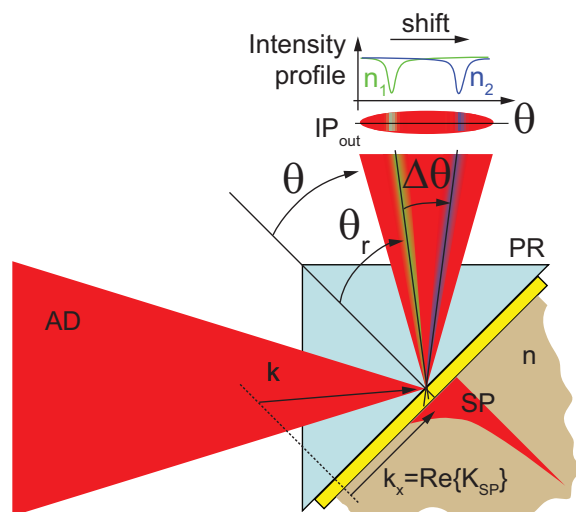
Fig. 1. SPR obtained with angular modulation of the horizontal wavevector of the excitation light. At the angle of resonance θ_r, resonant transfer of energy occurs between the light and the SP, which induces a minimum in the intensity pattern (resonance dip shown in the green profile) of the reflected field (IP$_{out}$). If the refractive index n varies from n_1 to n_2, the resonance dip shifts accordingly to a new angle of resonance $\theta_r + \Delta\theta$. PR, metallized prism; AD, angular distribution of light; IP$_{out}$, intensity profile after the prism (cross-section).

Simulations

At a wavelength of 4.4 μm, transfer matrix simulations performed with a free software package [16] show a theoretical resonance angle of about $\theta_r = 45.7°$ with respect to the surface normal (Fig. 2). The selected values for the complex dielectric constants are presented in Table 1 where the value for CaF$_2$ was taken from [17] and the values for Ti and Au layers were taken from [18]. We attributed a refractive index value n=1 to the measured medium in our numerical simulations.

The width at half maximum is about 0.2°, which is narrower than the width of a resonance dip obtained in the visible region for a similar configuration. For example, the calculated width of the resonance dip for a 50 nm gold layer on a glass prism at a wavelength of 633 nm is about 0.6° [19]. As the detection area of infrared detectors is bigger than the one of detectors operating in the visible, care must be taken in order to resolve the resonance dip efficiently.

Table 1. Layer parameters for CaF$_2$-Ti-Au structure

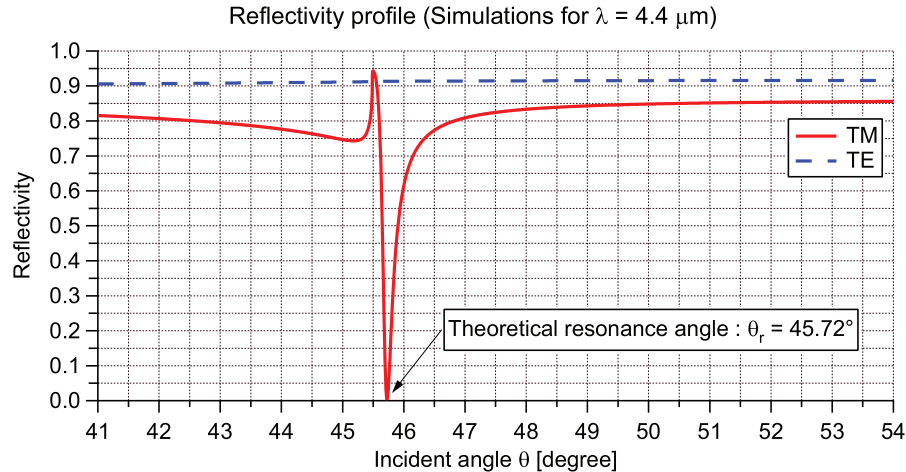| Material	Layer thickness [nm]	$Re\{\varepsilon\}$	$Im\{\varepsilon\}$
CaF$_2$	–	1.977	0
Ti	3	-41	7.35
Au	14	-700	60.698
Air	–	1	0

Reflectivity profile (Simulations for λ = 4.4 μm)

Fig. 2. Transfer matrix simulation for a 3 nm Ti and 14 nm Au multi-layer structure on a CaF$_2$ prism for mid-IR light excitation at 4.4 μm.

Mid-IR optical setup description

A schematic diagram of the design of the mid-IR SPR sensor is shown in Fig. 3(a). As mentioned before, the experimental setup was based on a Kretschmann geometry with Ti/Au thin layers directly deposited on a CaF$_2$ prism. This coupling device was mounted on a measurement cell where different gas specimens could be injected in and optically probed by the surface plasmon. The mid-infrared polarized source used for SP excitation was a QCL operating at 4.4 μm wavelength in pulsed regime with a duty cycle of 5%. The laser was mounted on a Peltier cooler and kept at a temperature of $-20\,^\circ$C. Due to the high divergence of the source, the laser beam was sent directly through the prism onto the metal-analyte interface with a 10° angular-distribution around the predicted resonance angle (45.7°). This means the laser beam was not focused on the prism-metal interface as shown in Fig. 1. In order to modify the illuminating conditions, the prism could be horizontally rotated and vertically translated. The signal intensity was rapidly decreasing after the prism and was horizontally recovered with a ZnSe cylindrical lens mounted horizontally near the exit facet of the prism (Fig. 3(b)). At the image location, the intensity pattern was an horizontal line, which was measured by x-z step scanning with a room temperature HgCdTe detector (detection area : 1 mm^2) mounted on two motorized translation stages and connected to a lock-in amplifier. The polarization of the laser beam was selected by rotating the QCL source along its optical axis exploiting the intrinsic TM-polarization of the QCL intersubband transitions [20].

In order to test the sensing capability of the system, CO$_2$ and N$_2$ mixtures were used as test samples. Different CO$_2$ concentrations were injected in the measurement cell and the position of the resonance dip was measured accordingly. For this purpose, the measurement cell was connected to a gas mixing device designed in order to obtain mixtures of different gases whose proportions were set by partial pressure measurements.

3. Experimental results

3.1. Evidence of SPR phenomena

The experimental intensity patterns and profiles with air as probed medium are shown in Fig. 4 for different polarizations. These measurements were done with D$_1$ = 21 cm and D$_2$ = 5 cm
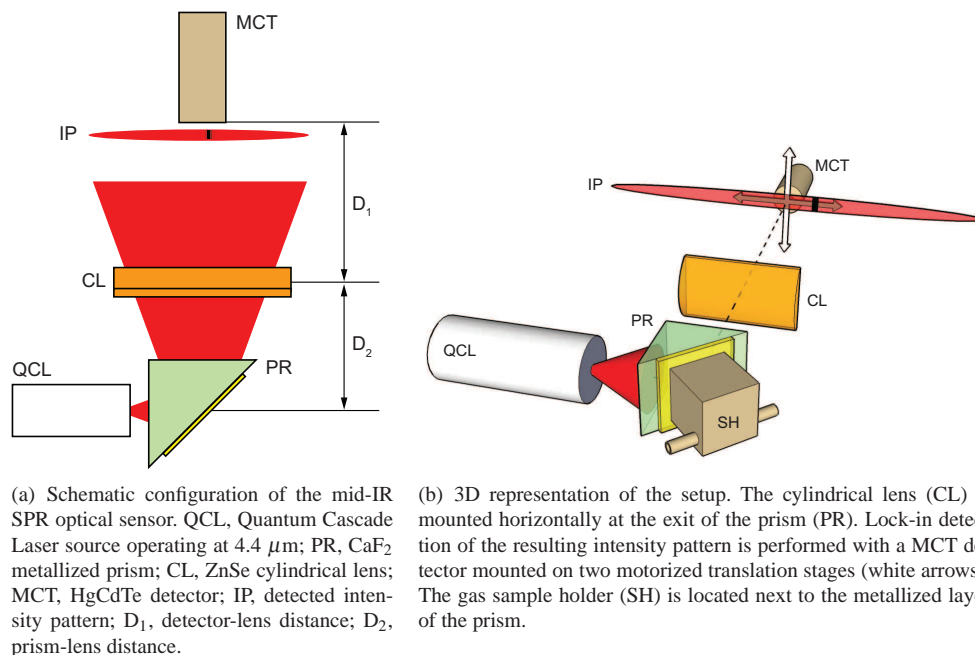
(a) Schematic configuration of the mid-IR SPR optical sensor. QCL, Quantum Cascade Laser source operating at 4.4 μm; PR, CaF$_2$ metallized prism; CL, ZnSe cylindrical lens; MCT, HgCdTe detector; IP, detected intensity pattern; D$_1$, detector-lens distance; D$_2$, prism-lens distance.

(b) 3D representation of the setup. The cylindrical lens (CL) is mounted horizontally at the exit of the prism (PR). Lock-in detection of the resulting intensity pattern is performed with a MCT detector mounted on two motorized translation stages (white arrows). The gas sample holder (SH) is located next to the metallized layer of the prism.

Fig. 3. mid-IR SPR optical sensor representations.

as shown in Fig. 3(a)). The intensity distribution obtained with TM polarization is shown in Fig. 4(a) and the intensity profile obtained along the dotted line shown in Fig. 4(a) is shown in Fig. 4(b). The intensity pattern was slightly inclined on the left due to alignment of the optical setup. The intensity pattern shows a vertical line located at 46.1° which is represented by a clear dip in the intensity profile. While the polarization of the excitation beam was rotated, the vertical line progressively disappeared (Fig. 4(c) and 4(d)). When the polarization was set to TE, there was no more vertical line on the intensity pattern (Fig. 4(e)) and the associated dip disappeared accordingly (Fig. 4(f)). As predicted by simulations, the dip was visible only for TM polarization, which indicates that the loss of intensity located at 46.1° on Fig. 4(a) was due to SPR. The loss of contrast between the simulations (Fig. 2) and the measured intensity profile (Fig. 4(a)) is due to the finite detector size (1mm x 1mm).

Rotating and translating the prism allowed to show that the vertical line obtained in the TM polarization was not due to artefacts of the optical setup. These operations modified the illumination conditions. When the prism was horizontally rotated, the incident angle of the light impinging on the gold layer was modified. This operation did not change the value of the resonance angle (46.1°), but the vertical line was horizontally translated in the plane of the detector with the same direction as the rotation of the prism. When the prism was vertically translated in order to select another illuminated area of the gold layer (same incident angle), the position and the size of the vertical line remained the same. This shows that the gold layer thickness was homogeneously distributed.

3.2. Results with gas measurements

The cell holding the CaF$_2$ prism allowed to change the measured medium next to the Ti/Au layer structure. N$_2$ and CO$_2$ were alternatively injected into the cell before the measurements. In a first step, 2D intensity patterns were measured to ensure that they were not vertically

(a) Measured intensity pattern for TM polarization

(b) Intensity profile for TM polarization

(c) Measured intensity pattern for mixed polarization

(d) Intensity profile for mixed polarization

(e) Measured intensity pattern for TE polarization

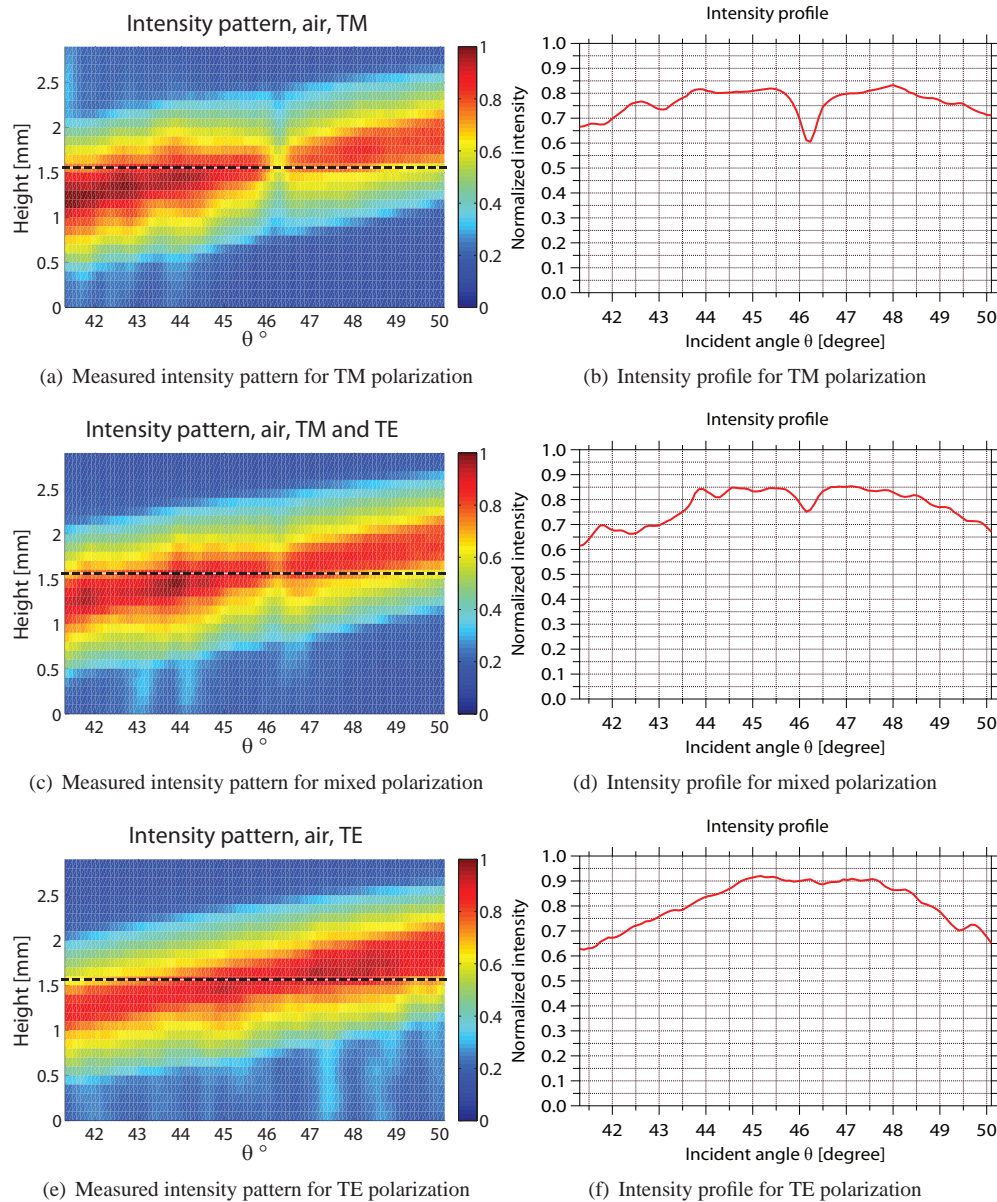(f) Intensity profile for TE polarization

Fig. 4. Intensity patterns and profiles for TM, mixed and TE polarizations when $D_1 + D_2 = 26$ cm. For details, see text.

moving due to mechanical deformations. Afterward, the intensity profiles were scanned (1 line scanning) with a total scanning time of no more than 2 minutes. The intensity profiles obtained for both gases are shown in Fig. 5. These measurements were performed with $D_1 = 4$ cm and $D_2 = 51$ cm (see Fig.3(a))
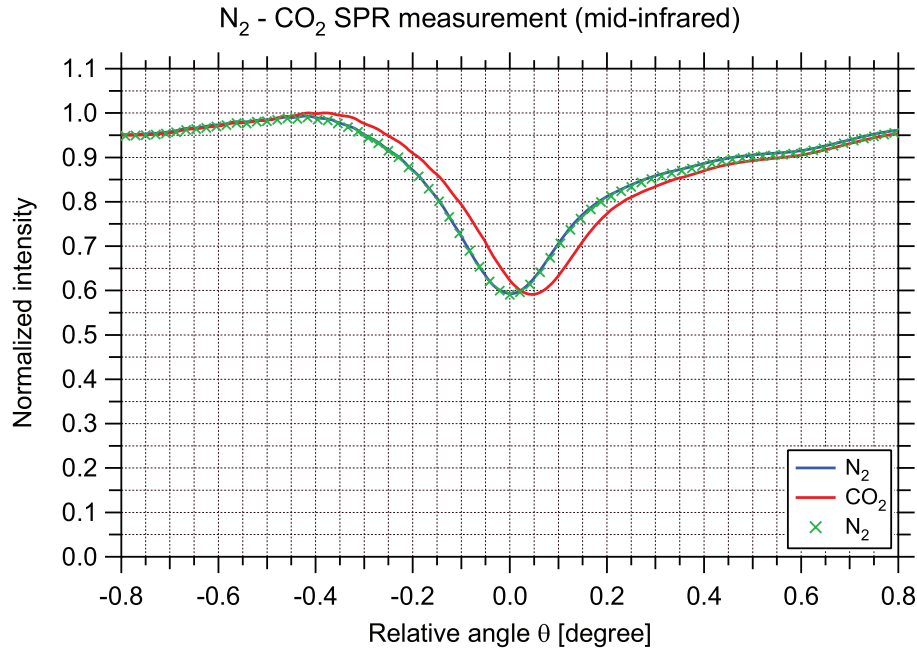

Fig. 5. Intensity profiles obtained for N_2 and CO_2 measurements. The resonance dip is shifted of $+0.045°$ when CO_2 is measured. This measurement is performed with $D_1 + D_2 = 55$ cm. The blue curve shows the measurement of N_2 before CO_2 and the green crosses show the measurement of N_2 after CO_2.

These measurements show an angular shift of $+0.045°$ with a repeatability of $+0.002°$ between N_2 and CO_2. Repeatability is illustrated by the green crosses, which show the N_2 measurement performed after the CO_2 measurement and the purge process.

In order to determine the sensitivity and the detection limit of this SPR-based sensor, various N_2-CO_2 mixtures have been measured. A CO_2 test sample has been progressively diluted with N_2 in order to divide the CO_2 concentration by two at each measurement. The experimental calibration curve, shown in Fig. 6, is obtained by measuring the position of the lower extremity of the resonance dip for each CO_2 concentration (red data). A linear interpolation of this experimental data shows a sensitivity of $S = 0.0005 \frac{deg}{\%CO_2}$ (black data). Variations of CO_2 below 2% cannot be clearly detected. This limitation is caused by the poor gas mixing accuracy achievable with our mixing device.

Nevertheless, these results show that the amplitude of the shift of the resonance dip is due to the variation of concentration of CO_2 in N_2.

In order to measure the sensitivity enhancement due to absorption in the mid infrared range, the same N_2 and CO_2 measurements have been performed with a visible SPR optical sensor at a wavelength of 633 nm (Fig. 7(a)). In this situation, a TM-polarized angular distribution of light impinging on a gold layer with a dielectric protective layer optimized for the visible range at 633 nm was reflected and measured with a CCD line camera. The prism-detector distance D_3 was 17 cm. In this configuration, the resonance angle θ_r was $46.2°$ and the full width at
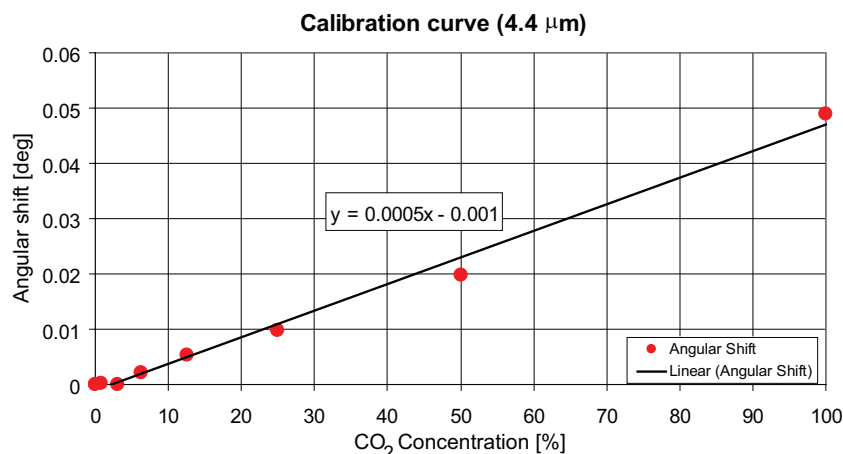
Calibration curve (4.4 µm)

Fig. 6. Measured sensitivity with mixtures of CO_2 in N_2. The CO_2 concentration is divided by two at each measurement (red points). The sensitivity is the slope obtained for the linear fit (black line).

half maximum (FWHM) was 2.2°, which was significantly wider than what is observed in the mid-infrared. According to [21], the refractive index variation between N_2 and CO_2 for a wavelength of 633 nm at atmospheric pressure and ambient temperature is 1.36×10^{-4} RIU. For this variation, transfer matrix simulations give a theoretical angular shift of $\Delta\theta = 0.0066°$ for a SPR sensor designed at a wavelength of 633 nm where no absorption occurs.
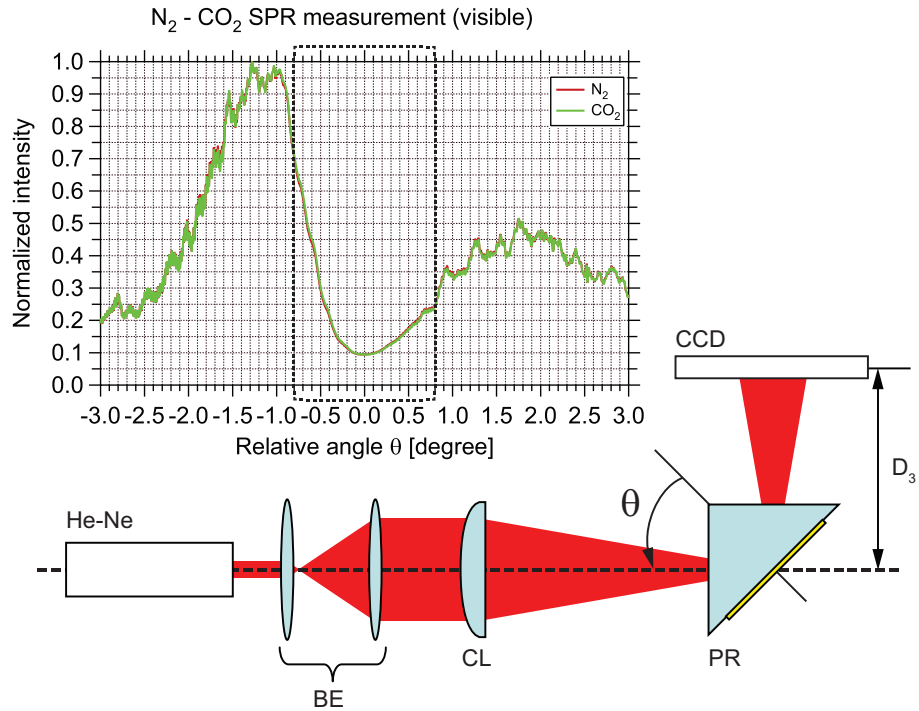
The resonance dip profiles obtained for CO_2 and N_2 with this configuration are shown in the inset of Fig. 7(a). The more detailed view located in the dashed rectangle is shown in Fig. 7(b). This figure allows to compare measurements performed in the visible range (brown and green curves) with the ones performed in the mid-infrared range (blue and red curves shown in Fig. 5). The angular shift of the measurement performed in the visible is $< +0.01°$ and is not clearly observable, which agree very well with the simulations performed for the visible case. Chemisorption or physisorption properties for CO_2 and N_2 at the sensor surface could explain the observed sensitivity increase. However, as shown in [22], this can be ruled out, since no evidence for such a mechanism has been found in the case of CO_2.

Since the angular shift is almost $+0.05°$ in the mid-infrared in the same configuration, a 5-time sensitivity enhancement is obtained with mid-IR SPR.

Work is in progress to increase the sensitivity by selecting a better excitation wavelength in order to fully exploit the absorption properties of CO_2. This should be obtained with a tunable QCL source [23] able to select wavelengths around a wavelength of 4.4 µm. Scanning process will be performed faster by replacing the moving one-pixel detector with an array of IR detectors.

4.   Conclusions

A plasmonic resonance has been successfully observed in the mid-infrared range at a wavelength of 4.4 µm. The experimental setup is based on a Kretschmann geometry with Ti/Au layers directly deposited on a CaF_2 prism. Evidence for surface plasmon resonance has been demonstrated and gas measurements have been performed in order to show that the sensitivity is higher in the mid-infrared range than in the visible. Work is in progress to implement a suitable mid-IR tunable source in order to fully benefits the absorption properties of CO_2. This will

N$_2$ - CO$_2$ SPR measurement (visible)

(a) Schematic configuration of the visible SPR optical sensor. He-Ne, polarized He-Ne laser source operating at 633 nm; BE, beam expander; PR, metallized glass prism; CL : cylindrical lens; CCD, CCD line detector; D$_3$, prism-detector distance. The inset shows the measurements of N$_2$ and CO$_2$ performed with this configuration. The more detailed view located in the dashed rectangle is shown in Fig. 7(b).

N$_2$ - CO$_2$ SPR measurement (infrared and visible)
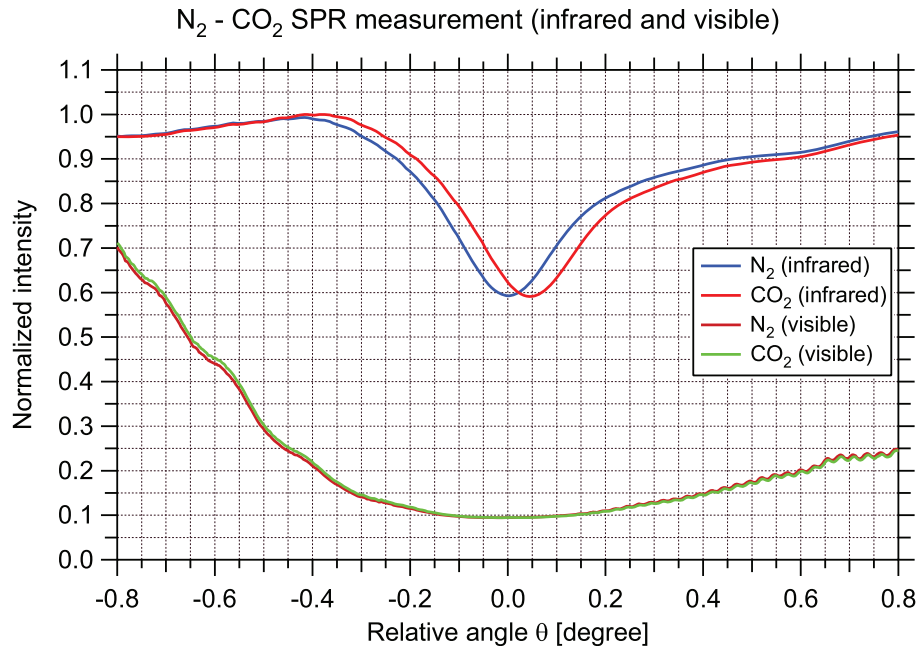
(b) Intensity profiles obtained for N$_2$ and CO$_2$ measurements at a wavelength of 633 nm (brown and green curves) and at a wavelength of 4.4 μm (blue and red curves shown in Fig. 5).

Fig. 7. Comparison between N$_2$ and CO$_2$ measurements performed in the visible (633 nm) and the mid-infrared range (4.4 μm).

allow to find the suitable wavelength to get the maximum sensitivity for CO_2 detection.